Three-Dimensional Modelling of Slab-Track Systems Based on Dynamic Experimental Tests

D. Thölken[1,2,3], J.E. Abdalla Filho[3], J. Pombo[4,5], J. Sainz-Aja[6], I. Carrascal[6], J. Polanco[6], A. Esen[7], O. Laghrouche[7], P. Woodward[8]

[1]*Mechanical Engineering Graduate Program, Pontificia Universidade Catolica do Paraná, Brazil*
[2]*Civil Engineering, Universidade Tuiuti do Paraná, Brazil*
[3]*Civil Engineering Graduate Program, Universidade Tecnologica Federal do Paraná, Brazil,*
[4]*Institute of Railway Research, University of Huddersfield, UK*
[5]*IDMEC, Instituto Superior Técnico, Universidade de Lisboa, Portugal and ISEL, IPL, Portugal*
[6]*LADICIM (Laboratory of Science and Engineering of Materials), University of Cantabria, Spain*
[7]*School of Energy, Geoscience, Infrastructure & Society, Heriot-Watt University, UK*
[8]*Institute for High Speed Rail and System Integration, University of Leeds, UK*

ABSTRACT

The accurate computational modelling of railway systems is crucial for analysis and design, which allows for excellent and enduring performance of such systems. It is capable of providing the industry with data for improving speed, comfort, load capacity and reliability. Further, as accurate solutions serve as an aid to improve railway systems, they contribute to quality services, social welfare, cost effectiveness and sustainability. An important component of a railway system is the track, which, in general, requires high investments for construction and maintenance. This work develops calibrated three-dimensional (3D) Finite Element (FE) models for slab track systems which can be employed for analysis and design with great level of reliability. These models are developed based on full-scale dynamic tests performed under the application of loads which simulate the passage of high-speed trains. The components considered are the rails, rail pads, slab track, grout, Hydraulicaly Bonded Layer (HBL), Frost Protection Layer (FPL) and subgrade. The FE models are built and calibrated in order to reproduce the measured displacement and acceleration test results. Due to the uncertainties in some material properties, a parametric analysis is also performed to establish to which material characteristics of the system the model is more sensitive to. It has been found that the Young's moduli for the FPL layer and subgrade are the most important parameters. Further, the stiffness properties of rail pads play a paramount role in the accuracy of the model.

Keywords: Railway Dynamics, Slab-Tracks, Full-Scale Tests, Dynamic Finite Element Modelling, Parametric Analysis.

1. Introduction

Research development and industrial progress in railway engineering are relevant to lever a nation's economy in general. Specifically, they contribute to safer, faster and more reliable transportation systems of people and cargo, freeing space in highways as the requirement for trucks and passenger cars becomes unavoidably lower. Further, the railway modal is more environmentally friendly, which is an important world asset. Compared to highway and air transportation modes, the railway mode presents lower costs, lower energy consumption and lower CO_2 emissions, which contribute favourably to the climate change problems that the world currently faces. Combined with these factors, there are also advantages in terms of comfort, safety and mobility that are highlighted in many countries to justify the investment in this mode of transport. These developments are seeking to optimize the rail systems in terms of speed, capacity and comfort, and to reduce operational and maintenance costs. In large developing countries, such as Brazil and India, the railway system needs to be improved to allow for more efficient transportation of people and cargo, which would be beneficial to the economy and to the environment.

One of the main lines of research in railway engineering is the modelling of the dynamic interaction between vehicles and rail infrastructure. This topic has been investigated over the past few decades and, as the use of high-speed trains increases worldwide [1], vehicle-structure dynamic interaction has grown in importance. Results provided by accurate models contribute to improve the design of both vehicles and track systems, offering useful information for maintenance protocols, and contribute for more efficient use of resources that consequently will reduce life cycle costs.

There are several types of tracks technologies [2], being ballast track [3–7], slab track [8–11] and ballast-with-asphalt track [12,13] the most common examples. The study of the track structure conditions and of its dynamic performance has devoted the attention of many researchers aiming to support the rail industry [14–20]. Numerical models have been developed mainly using Multibody (MB) and FE methodologies. In some cases, the track is considered as a periodic elastically coupled beam system resting on flexible foundations [21–23]. Other authors have proposed to study the train-track system with different levels of complexity and analysis goals [24–28]. Cai and Raymond developed a three-dimensional model including coupled spring-dashpot elements to analyse the behaviour of rail pads, ties and ballast [21]. Nguyen *et al.* did a comparison between 2D and 3D models considering the performance of rail pads modelled as spring and damper elements [29]. Sainz-Aja *et al.* studied experimentally the properties of rail pads under different operational conditions [30]. Other authors have proposed co-simulation methodologies between MB and FE formulations in order to study the track structure under realistic trainset loads [31–34]. These developments open the possibility of integrating complex track geometries [35–37], more detailed wheel-rail contact models [38–46], to consider track irregularities [47,48] and other track singularities [49–51] in the studies aiming to assess the track performance and degradation evolution [52–57] in realistic operation conditions.

In general, the slab track system is composed of precast concrete slabs with embedded concrete sleepers, which hold the pads and clips (fastening system) to support and fix the rails. The substructure underneath the slabs is composed of layers of different materials. From top to bottom, these layers are the HBL, FPL and subgrade. The HBL is a mixture of soil, water and cement while the FPL is a compacted permeable soil [58]. On the other hand, the ballast track system employs gravel which is laid on subgrade. Then, evenly spaced sleepers are transversely positioned on the gravel to support the rails through pads. The ballast-with-asphalt track system uses an asphalt layer laid on subgrade before the ballast layer is placed. Then, sleepers, pads and rails are assembled [59]. The two types of track systems most widely used are the slab track and ballast track systems. The latter is not very adequate for increased train speeds [58,60]. The study presented here investigates the behaviour of a slab track system.

The slab track with embedded sleepers have been widely used as an alternative for non-ballast tracks. The literature shows that the system has been studied in many aspects in order to be used as an efficient railway track system [6,9–11,58,59,61–63]. Research and practice indicate that slab track systems may have problems with temperature, train loads and subgrade settlements [64]. Occurrence of transverse-through cracks is particularly one of the principal hazards in short-term operation [65]. However, it offers greater stability and less sensitivity with the unevenness of the lower layers [58,59,61]. Another important aspect to consider in railway projects is the cost. If a slab track system requires high initial investments [62,63], consideration of its life cycle costs indicates that it is a very competitive system, being one of the reasons for its implementation [66]. For instance, in France, the solution New Ballastless Track (NBT) was designed considering a 100 year-operation period without substantial maintenance, subjected to train velocities up to 360 km/h and axle loads up to 250 kN. The project considered a depreciation period of 10-25 years [67].

The main objective of this work is to develop reliable 3D FE models of a slab track system based on a full-scale prototype that has been extensively tested in laboratory. Then, the purpose is to identify

the material properties to which the model behaviour is more sensitive to via a parametric analysis. ABAQUS software is here used for FE modelling. The experimental results are used as reference to calibrate the FE models and, ultimately, to validate the proposed methodologies. For this purpose, several realistic dynamic load scenarios are considered. Once the slab track models are calibrated, a parametric analysis is performed in order to identify the material properties that have higher influence in the dynamic performance of the rail infrastructure. The results will enable to conclude which physical/mechanical parameters need to be assessed with higher accuracy in the dynamic analysis of railway track systems. The successful conclusion of this work opens the possibility to study vehicle-infrastructure interaction using detailed and reliable track models. These studies can be performed in realistic operation scenarios in order to assess the dynamic behaviour of trains and to predict the long-term performance of the infrastructure. The results of such studies can contribute favourably to the railway industry by promoting the development of advanced technological solutions aiming to reduce the life cycle costs of tracks and the vehicle maintenance needs.

2. Full-Scale Experimental Tests

This section presents the experimental apparatus and the full-scale testing used in this work. The experimental results provide reference values to calibrate the FE models for track analysis.

2.1. GRAFT II Test Facility

The full-scale tests are performed on a physical model of a slab track using the testing facility known as GRAFT II (Geo-Pavement and Railways Accelerated Fatigue Testing) which is located at Heriot-Watt University in Edinburgh, Scotland. Full-scale testing of slab and ballast tracks under phased cyclic loading using GRAFT II is described in [68]. GRAFT II is one of the world largest purpose-built laboratory track bed designed to predict the effects of trains on the track. Figure 1 shows a frontal view of the apparatus which clearly depicts the slab track system, the steel frame and the actuators. In more detail, the picture shows six UIC 60 rail pieces that are 40 cm in length to allow for complete load control in each actuator. Also, the picture shows the precast concrete slab with embedded sleepers, the grout layer, the HBL, which is made of concrete, and the FPL and subgrade, both made of compacted sand. The grout layer connects the precast concrete slab to the HBL with the purpose of avoiding stress concentration points between the two concrete layers. Figure 2 represents another view of the test apparatus, which shows actuators and LVDT displacement sensors, where LVDT stands for Linear Variable Differential Transformer.

Figure 1 – GRAFT II test facility– Slab track system

Figure 2 – GRAFT II test facility - Actuators and LVDTs

Figure 3 shows a schematic representation of the cross-section view as well as a longitudinal view of the slab track system, both including all relevant dimensions and the six positions of the load application by the actuators onto the sleepers. The figure also clearly depicts the five different track material layers, which have already been described.

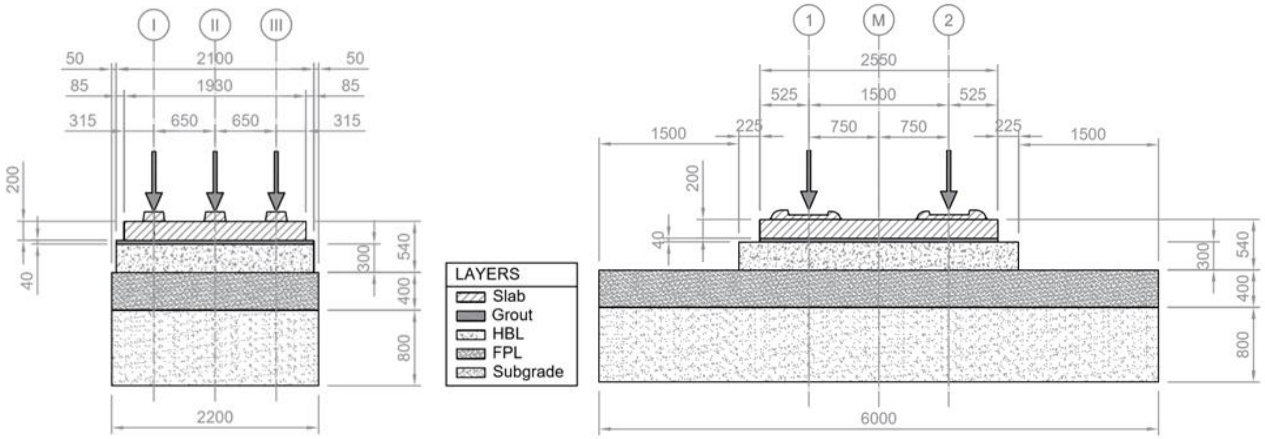

Figure 3 – Cross section and longitudinal views of the slab track system (dimension units: mm)

The test apparatus has one actuator on the top of each of the six rail parts for load application, as shown in Figure 4(a). There are eight displacement sensors (LVDTs) in the experimental test as shown in Figure 4(b). Four of them are placed on the top of sleepers and four are placed on the top of rails, in the same positions of actuators 1 to 4, which are represented by ACT_1, ACT_2, ACT_3 and ACT_4 in the figure. The four sensors which are installed on sleepers are represented by LVDT_1, LVDT_2, LVDT_3 and LVDT_4.

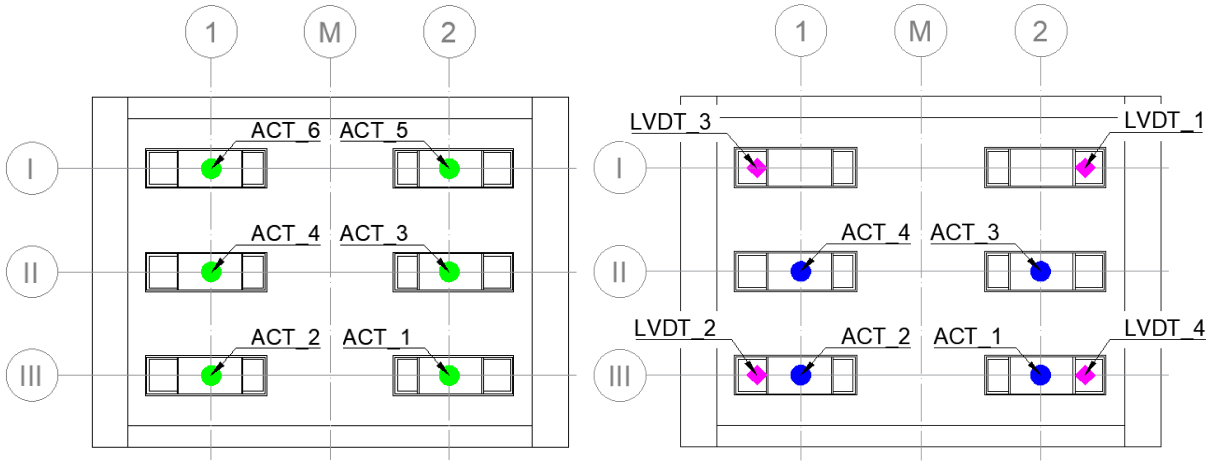

Figure 4 – a) Actuators; b) displacement sensors positions

The loads are applied first statically and then dynamically. Thus, loadings are arranged in groups of static cases and dynamic cases. The static study has three scenarios; namely, (i) Scenario 1 with a total of 13 ton load distributed on the three sleepers with percentages of 25%, 50%, and 25%, respectively; (ii) Scenario 2 with a total of 17 ton load distributed on the three sleepers with percentages of 25%, 50%, and 25%, respectively; and (iii) Scenario 3 with a total of 25.8 ton load evenly distributed on the three sleepers. Figure 5(a) shows the representations of scenarios 1 and 2, while scenario 3 is depicted in Figure 5(b). Figure 5(c) shows the plan view representation of these static load distributions.

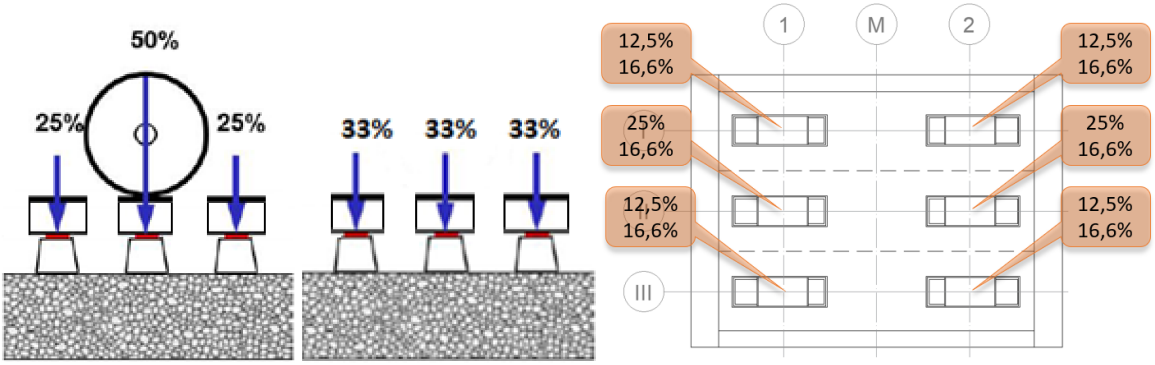

Figure 5 – Static load distribution: a) Scenarios 1 and 2; b) Scenario 3; c) Plan view

The dynamic study is divided in two scenarios with different load frequencies. They are named Scenario 4, whose load frequency is 5.6 Hz, and Scenario 5, whose load frequency is 2.5 Hz. Each scenario is subdivided in a given number of steps according to the load application procedure. Scenario 4 has three steps; namely, Sc4-1 with 3.7 ton, Sc4-2 with 7.2 ton, and Sc4-3 with 9.5 ton. Scenario 5 has four steps; namely, Sc5-1 with 4.0 ton, Sc5-2 with 7.9 ton, Sc5-3 with 11.7 and Sc5-4 with 15.8 ton. The loads are applied in full at the three sleepers in different times. That is, 100%, 100% and 100% in each sleeper as shown in Figure 6(a). Figure 6(b) shows the plan view of this load application procedure, depicting that the load is applied equally by each wheel at a given time.

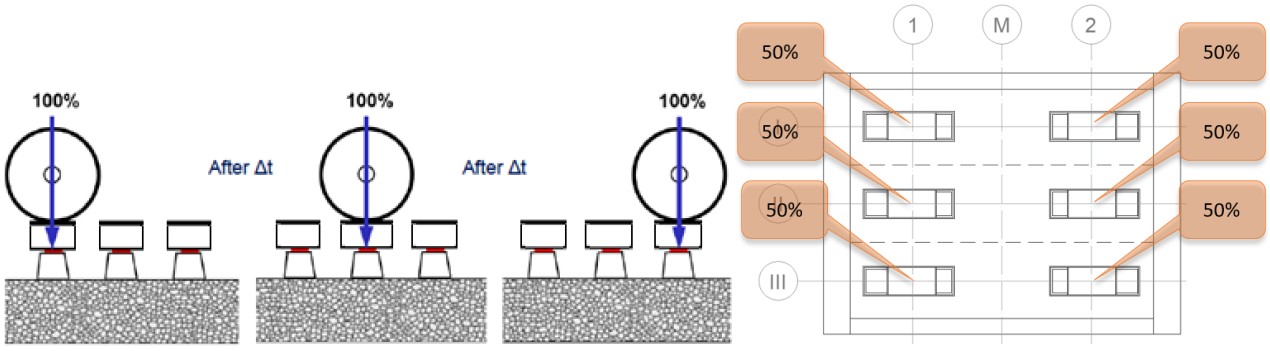

Figure 6 – Dynamic load distribution: a) Scenarios 4 and 5; b) Plan view

The frequency of the dynamic loads corresponds to train speeds of 360 km/h and 160 km/h, respectively, in Scenario 4 and 5. These two speeds are important because high-speed and conventional speed trains can operate in the same tracks. The time lag between load applications on each sleeper is an experimental test input, as well as the distance between sleepers, which is 0.65 m. Another relevant input parameter is the distance between bogies for high-speed trains, which is considered here as 18 m. This information allows for the definition of the load application time lag used in the experiments.

2.2. Rail Pads Characterization

Fastening system is one of the most important elements in the maintenance and durability of the railway superstructure [69]. One of the most important elements within the fastening system is the rail pad, whose main functions are to provide flexibility to the track and impact attenuation. The fastening system used in full-scale tests is the Vossloh 300, which is composed by different layers. The first layer is made of EVA (Ethylene Vinyl Acetate), which is an elastomeric polymer. Then, a steel plate and finally a layer of EPDM (Ethylene Propylene Diene Methylene), which is a rubber. In case of EVA and EPDM components, they are highly non-linear materials, so their mechanical properties will depend on the load values to which they are subjected [30]. Estimating the mechanical response of the rail pads based on the test conditions is a complex task [70]. For this reason, laboratory tests on rail pads identical to those used in the full-scale test were carried out using the corresponding values of load and frequency. In the FE model, the fastening system is considered as a single element, so equivalent properties are defined to produce a similar behaviour in the equivalent element as in the entire fastening system. The calibrated equivalent Young's modulus values (E_{eq}) for static and dynamic studies considering an equivalent single-layer rail pad are listed in Table 1. The values are different for the lateral and middle rail pads for static scenarios 1 and 2 because the loads are applied unevenly on them (25%, 50% and 25%), as shown in Figure 5(a).

Table 1 – Under rail pad Young's modulus

Scenario	Static Scenarios					Dynamic Scenarios						
	Sc1 Middle	Sc1 Lateral	Sc2 Middle	Sc2 Lateral	Sc3	Sc4-1	Sc4-2	Sc4-3	Sc5-1	Sc5-2	Sc5-3	Sc5-4
E_{eq} (MPa)	5.633	5.964	5.941	5.787	5.967	20.188	16.217	14.138	23.360	18.195	14.340	12.520

3. Slab Track Modelling

The slab track full-scale experimental tests, described in Section 2, are modelled in this section. The modelling procedure consists of the three steps, namely the structural modelling, FE modelling and FE analysis. The structural model includes a geometric representation of the problem (Figure 7), the definition of boundary conditions, material properties and loading. The FE modelling step adopts suitable FE types for the analysis and establishes an adequate mesh configuration upon a convergence study. Finally, the FE analysis step consists of the static and dynamic calibration of the model considering the different load scenarios previously described and suitable initial conditions to match the conditions of the physical tests. The data used in the FE modelling is listed in Table 2.

3.1. Structural Model

Figure 7 shows a geometric model of the slab track system, which includes rails, rail pads, the concrete slab, grout, HBL and FPL layers, and the subgrade. The dimensions defined in Figure 3 are used. Different colours represent different materials. Boundary conditions are defined in order to better represent the restricted body in the physical experiment. Thus, displacements are restricted on the walls and at the bottom, but rotations are released. Material properties are assigned to the different materials accordingly. Rails are considered as rigid bodies as their behaviour is not of interest here. As in the physical experiments, they serve to receive the loads, which are considered as applied pressures. The rail pads are composed of EVA, steel and EPDM materials, as mentioned before. The stiffness of those components have been tested in laboratory during the course of this research [9], and the results have been used here. It is also important to note that Young's moduli for FPL layer and subgrade have been defined in the present model during the model's calibration procedure. All data parameters described in this paragraph are listed in Table 2.

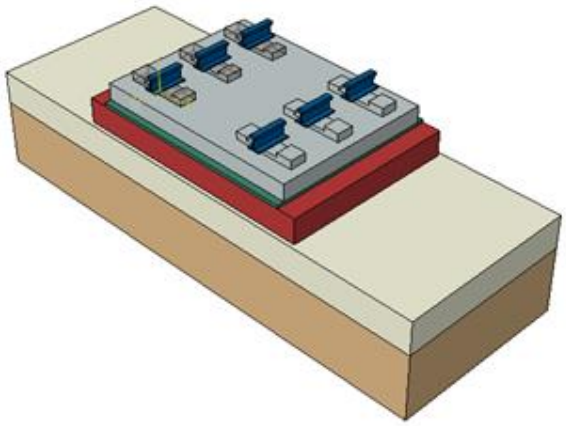

Figure 7 – Slab track system geometric model

Table 2 – Structural model parameters

Item	Condition
Displacement boundary conditions	Walls: Restricted Bottom: Restricted
Rotation boundary conditions	Walls: Free Bottom: Free
Layers compatibility	Nodal compatibility imposed (Tie connection function)
Load application	Pressure loading on the rails
Rail Properties	Density: 7850 kg/m³ Rigid Body Poisson's Ratio: 0.30
Under rail pad properties (EPDM+Steel+EVA)	Steel Plate: Density: 7850 kg/m³ Young's Modulus: 210.00 GPa EPDM and EVA: Young's Modulus tested in laboratory [9]
Concrete slab/sleepers properties	Density: 2500 kg/m³ Young's Modulus: 36.00 GPa Poisson's Ratio: 0.20
Grout properties	Density: 2300 kg/m³ Young's Modulus: 22.50 GPa Poisson's Ratio: 0.20
HBL properties	Density: 2400 kg/m³ Young's Modulus: 17.87 GPa Poisson's Ratio: 0.20
FPL properties	Density: 2144 kg/m³ Young's Modulus: according to the literature and calibration considering experimental tests and numerical models Poisson's Ratio: 0.30
Subgrade properties	Density: 2091 kg/m³ Young's Modulus: according to the literature and calibration considering experimental tests and numerical models Poisson's Ratio: 0.30

3.2. Finite Element Model

The slab track system structural model is discretized via 3D FE using ABAQUS software. The elements adopted are 8-node bricks, which are based on quadratic polynomials. The double symmetry of the structural model is recognized, and only one-quarter of that model is required for FE modelling. Compatibility between different material layers is guaranteed via the ABAQUS tie connection

function. A mesh convergence study is performed here in order to identify a mesh which can produce sufficiently accurate results without excessive computational costs. Uniform refinement is adopted because eventual stress concentrations that might occur are not of interest in this work. Cube elements are employed for simplicity and also for providing a good level of refinement in the first mesh. Convergence is considered to have been attained when the simple difference between displacement results from consecutive mesh refinements is not greater than 0.5%. Only three meshes end up being necessary in the mesh refinement study. These three meshes, which are shown in Figure 8, are built with 10 cm, 5 cm, and 2.5 cm elements, respectively.

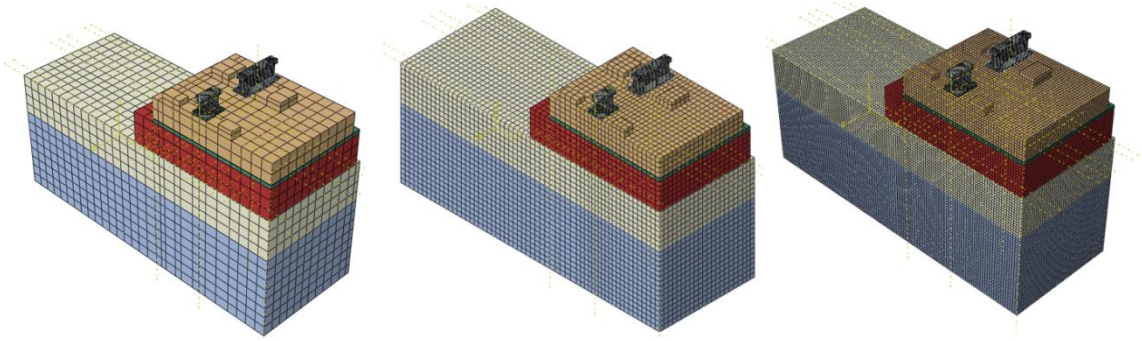

(a) 10 cm (b) 5 cm (c) 2.5 cm

Figure 8 – FE meshes: a) 10 cm-elements; b) 5 cm-elements; c) 2.5 cm-elements

Comparison of results provided by the 10 cm and 5 cm element meshes show an average difference of nearly 0.71%, whereas the average difference from the comparison between 5 cm and 2.5 cm element meshes is nearly 0.5%. Therefore, the intermediate mesh comprised of 5 cm elements has been considered adequate and, therefore, adopted for the static and dynamic analyses performed here.

3.3. Static Model Calibration

The calibration of the numerical models for static analyses are performed considering the parameters in Table 2 and the full-scale tests performed in laboratory. Table 3 contains the material properties of the rail pads and compacted sands (FPL and subgrade) adopted in the these studies, which are not defined in Table 2. The static numerical analyses use the average of displacement values acquired during a period of one second in order to avoid selecting a peak load displacement value. As it is a linear analysis, the settlement occurred during the time of the static load application is not considered.

Table 3 – Material properties used in the static model calibration

Layer	**Properties**
Equivalent Rail Pad (EPDM+Steel+EVA)	Young's Modulus (variable with load value) Sc1) Lateral sleepers: 5.963 MPa; Middle sleeper: 5.633 MPa Sc2) Lateral sleepers: 5.787 MPa; Middle sleeper: 5.941 MPa Sc3) Lateral sleepers: 5.967 MPa; Middle sleeper: 5.967 MPa
FPL	Density: 2144 kg/m³ Young's Modulus: 400 MPa Poisson's Ratio: 0.30
Subgrade	Density: 2091 kg/m³ Young's Modulus: 400 MPa Poisson's Ratio: 0.30

The objective of model calibration is to adjust the numerical model such that it is capable of reproducing with the best approximation possible the results provided by physical experiments. For this purpose, the target parameters are the displacements measurements taken at LVDTs (1, 2, 3 and 4) and actuators (1, 2, 3 and 4). The numerical results are compared to the experimental measurements for the three static load scenarios (Sc1, Sc2, Sc3) as shown in Figure 9. The 45-degree line represents

a perfect match between the numerical results and experimental values, which is the aim of the model calibration. Figure 9(a) describes the Actuators (ACT) displacements and Figure 9(b) describes the LVDT displacements. The proximity of the dots to the 45-degree line indicates that there is a good agreement between numerical and experimental results. The mean difference of the results shown in Figure 9 is nearly 10%. Taking into account that there are uncertainties in experimental data and approximations and limitations in the numerical models, this difference is considered acceptable and the numerical model is considered to be calibrated.

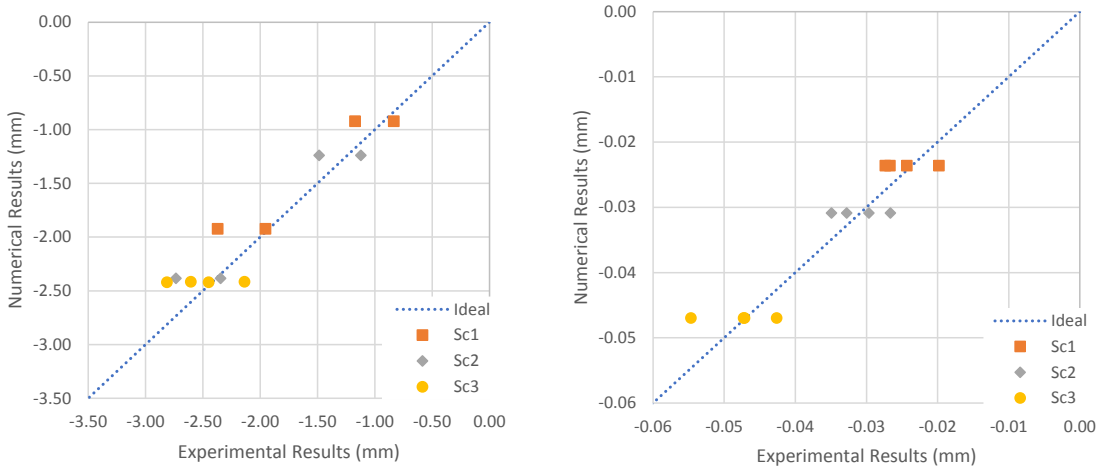

(a) (b)

Figure 9 – Static model calibration: a) Displacements at actuators; b) Displacements at LVDTs

3.4. Dynamic Model Calibration

The calibration of the numerical models for dynamic analyses are performed considering the parameters in Table 4 and the full-scale tests performed in laboratory. Table 4 contains the material properties of the equivalent rail pads and compacted sands (FPL and subgrade) adopted in these studies, which are not defined in Table 2. The dynamic analyses use smoothed displacement distributions which are obtained applying a Fourier regression analysis on the displacement set of values acquired from the LVDTs sensors. This is done so that there is a better agreement with the smoothed FE solutions provided by ABAQUS. Coefficients of Fourier series employed have 95% confidence bounds.

The 45-degree line graphs for the dynamic model calibration are shown in Figure 10 through Figure 17. In these figures, (a) presents displacement results and (b) contains acceleration results. Further, in each graph, EM refers to experimental measurements and NS to numerical solutions. The horizontal axes display the values of the amplitudes provided by the experimental measurements (EM), while the vertical axes display simultaneously the amplitudes of both the experimental measurements and numerical solutions (EM and NS). Figure 10 through Figure 13 show the results associated to the actuators, while Figure 14 through Figure 17 contain the results associated to the LVDTs. It can be seen that all graphs show that there is a good agreement between EM and NS results. The mean difference of displacement results is 9.06% with a standard deviation of 9.18%, while the mean difference of acceleration values is equal to 8.94% with a standard deviation of 9.12%. These results are considered to be good and the dynamic model is considered to be calibrated. It is relevant to mention that there are uncertainties associated to the measurements and in the soil parameters because those materials have not been tested.

Table 4 – Material properties used in the dynamic model calibration

Layer	Properties
Equivalent Rail Pad (EPDM+Steel+EVA)	Sc4-1: E = 20.188 MPa Sc4-2: E = 16.217 MPa Sc4-3: E = 14.138 MPa Sc5-1: E = 23.360 MPa Sc5-2: E = 18.195 MPa Sc5-3: E = 14.340 MPa Sc5-4: E = 12.520 MPa
FPL	Density: 2144 kg/m³ Young's Modulus: 500 MPa Poisson's Ratio: 0.30
Subgrade	Density: 2091 kg/m³ Young's Modulus: 500 MPa Poisson's Ratio: 0.30

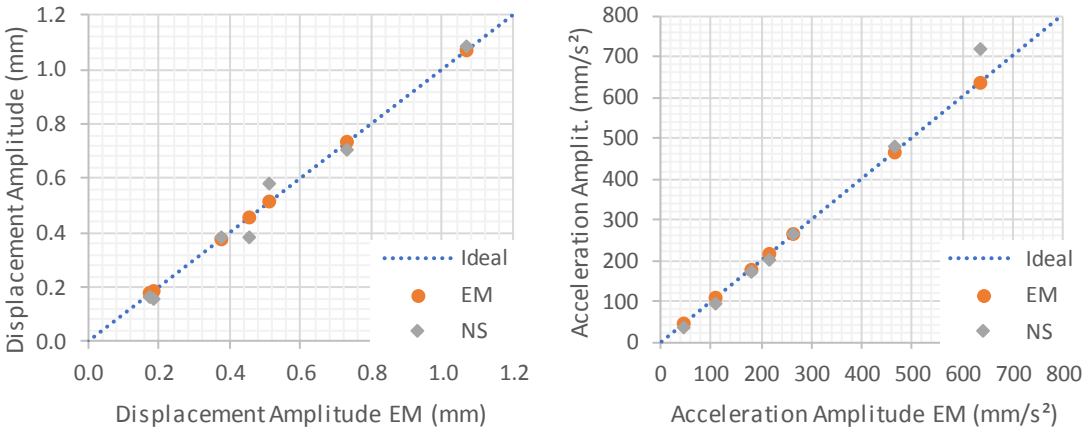

(a) Displacement (mm) (b) Acceleration (mm/s²)

Figure 10 – Dynamic model calibration for actuator 1

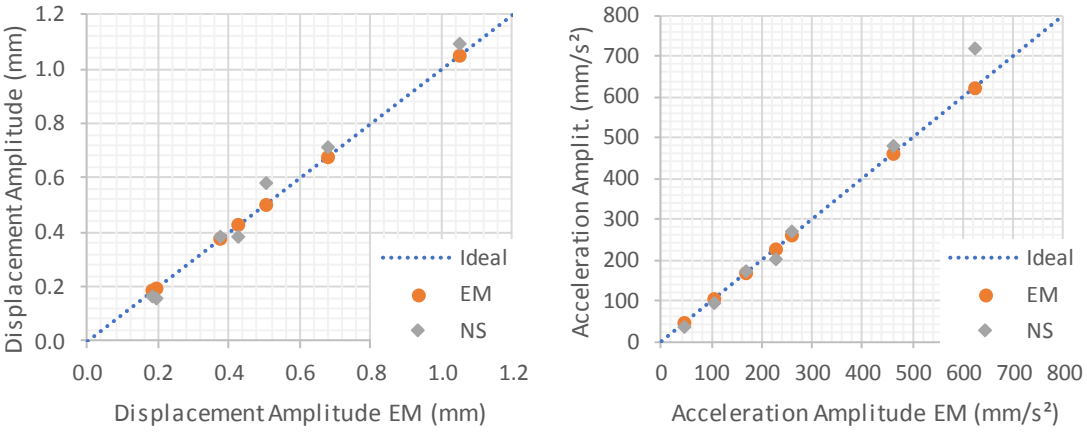

(a) Displacement (mm) (b) Acceleration (mm/s²)

Figure 11 – Dynamic model calibration for actuator 2

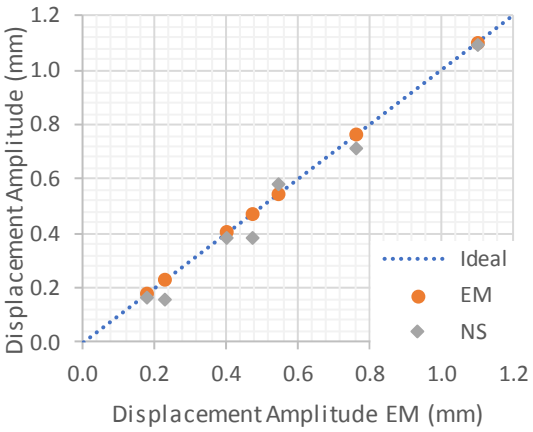

(a) Displacement (mm)

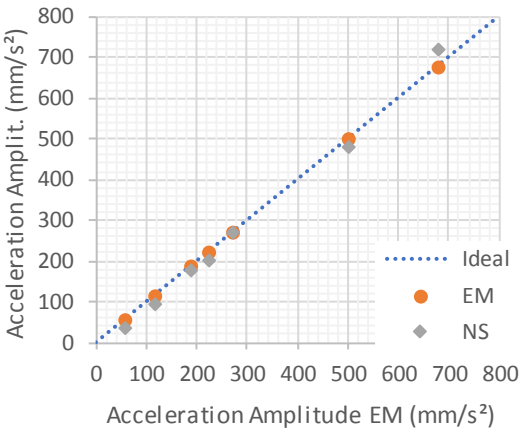

(b) Acceleration (mm/s²)

Figure 12 – Dynamic model calibration for actuator 3

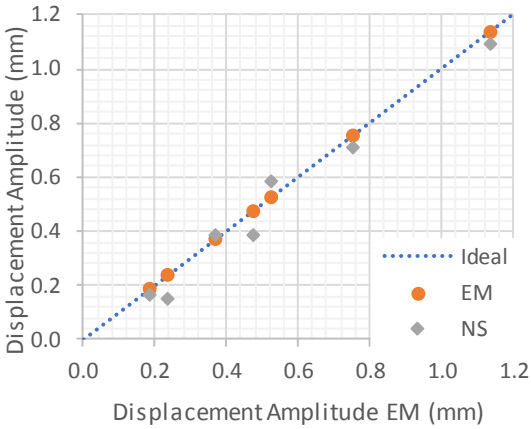

(a) Displacement (mm)

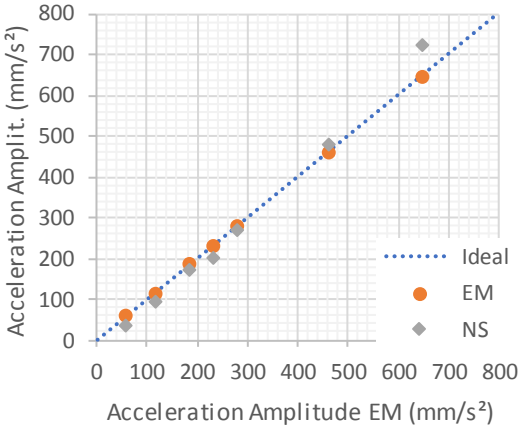

(b) Acceleration (mm/s²)

Figure 13 – Dynamic model calibration for actuator 4

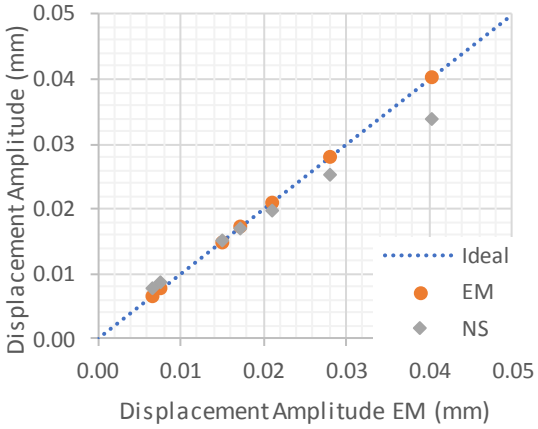

(a) Displacement (mm)

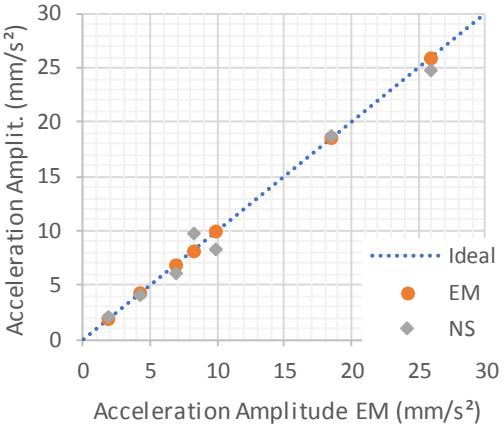

(b) Acceleration (mm/s²)

Figure 14 – Dynamic model calibration for LVDT 1

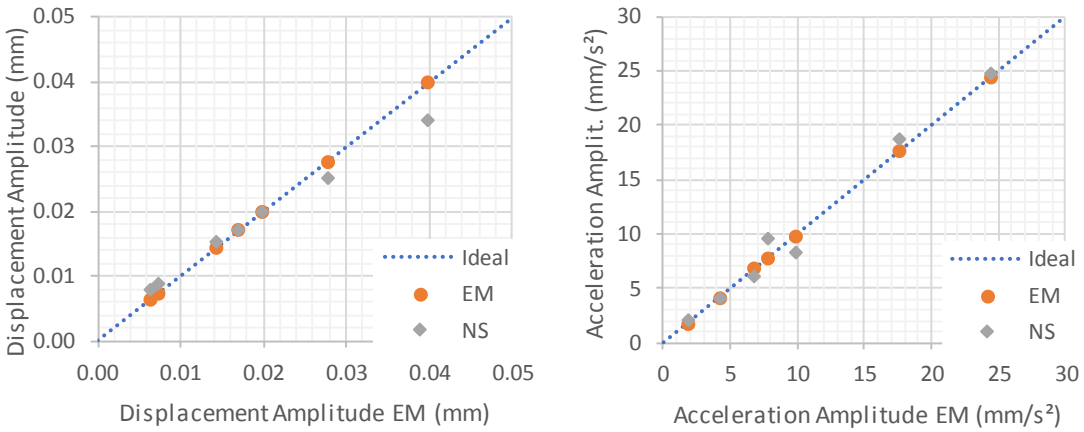

(a) Displacement (mm) (b) Acceleration (mm/s²)

Figure 15 – Dynamic model calibration for LVDT 2

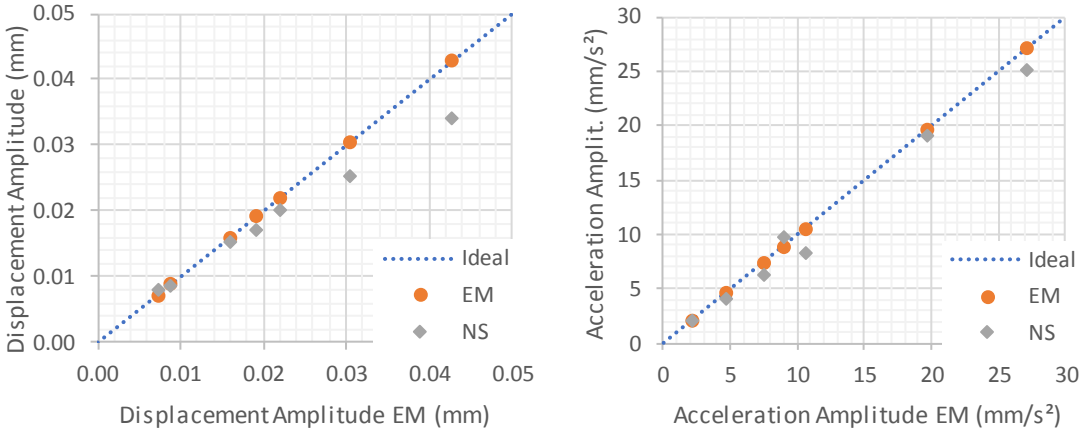

(a) Displacement (mm) (b) Acceleration (mm/s²)

Figure 16 – Dynamic model calibration for LVDT 3

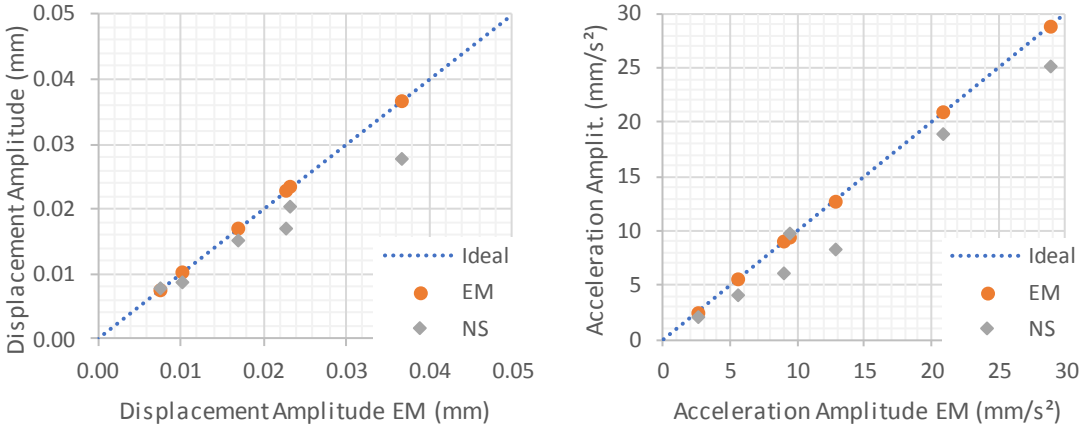

(a) Displacement (mm) (b) Acceleration (mm/s²)

Figure 17 – Dynamic model calibration for LVDT 4

4. Parametric Analysis

Static and dynamic FE models have been calibrated according to the data provided by the full-scale laboratory tests in Section 3. In this section, a parametric analysis is performed using those models in

order to identify which layers and material properties have the greatest influence on the behaviour of the slab track. Such an information will be useful to analysts who might use these or similar models to perform their own analyses. For conciseness, the parametric analysis is performed considering only the dynamic loading scenario Sc4-3 (see Section 2 for description). Effects in acceleration results of each layer of the model at the locations of the four actuators and the four LVDTs are evaluated using variations of -10% and + 10% in the values of density, Young's modulus and Poisson's ratio separately. Results are displayed in Table 5 through Table 10 showing the percentage variation of accelerations.

4.1. Density

Table 5 and Table 6 show the percentage variation of accelerations when density properties of the model's layers change -10% and +10%, respectively. It is seen that the variations are very close to zero, indicating that changes in density for this frequency range are not relevant in the model.

Table 5 – Accelerations variation for -10% change in density

Layer	ACT_1	ACT_2	ACT_3	ACT_4	LVDT_1	LVDT_2	LVDT_3	LVDT_4
Rail	0.00%	0.00%	-0.01%	-0.01%	0.01%	0.01%	0.02%	0.02%
Rail Pad	-0.01%	-0.01%	-0.01%	-0.01%	0.00%	0.00%	0.00%	0.00%
Slab	-0.01%	-0.01%	-0.01%	-0.01%	0.00%	0.00%	0.01%	0.01%
Grout	-0.01%	-0.01%	-0.01%	-0.01%	0.00%	0.00%	0.01%	0.01%
HBL	-0.01%	-0.01%	-0.01%	-0.01%	0.01%	0.01%	0.02%	0.02%
FPL	-0.01%	-0.01%	-0.01%	-0.01%	0.01%	0.01%	0.02%	0.02%
Subgrade	-0.01%	-0.01%	-0.01%	-0.01%	0.00%	0.00%	0.01%	0.01%

Table 6 – Accelerations variation for +10% change in density

Layer	ACT_1	ACT_2	ACT_3	ACT_4	LVDT_1	LVDT_2	LVDT_3	LVDT_4
Rail	-0.02%	-0.02%	-0.02%	-0.02%	-0.01%	-0.01%	0.00%	0.00%
Rail Pad	-0.01%	-0.01%	-0.02%	-0.02%	0.00%	0.00%	0.00%	0.00%
Slab	-0.01%	-0.01%	-0.02%	-0.02%	-0.01%	-0.01%	-0.02%	-0.02%
Grout	-0.01%	-0.01%	-0.01%	-0.01%	0.00%	0.00%	0.01%	0.01%
HBL	-0.01%	-0.01%	-0.02%	-0.02%	-0.01%	-0.01%	0.00%	-0.02%
FPL	-0.01%	-0.01%	-0.02%	-0.02%	-0.01%	-0.01%	0.00%	0.00%
Subgrade	-0.01%	-0.01%	-0.01%	-0.02%	0.00%	0.00%	0.01%	0.01%

4.2. Young's Modulus

Table 7 and Table 8 show the percentage variation of accelerations when the Young's moduli of the model's layers change -10% and +10%, respectively. It is seen that the more important variations occur with the changes in Young's modulus of rail pads, FPL and subgrade. Focusing on the rail pads, a 10% decrease in Young's modulus cause a decrease of 10.6% in accelerations at the actuator positions. Also 8.6% increase is registered when the Young's modulus increases 10%. Considering the FPL, the accelerations decrease nearly 7% and increase nearly 6% at the LVDT positions, respectively, with the 10% decrease and increase in Young's modulus. At these same positions, the accelerations in the subgrade decrease over 3% and increase nearly 3%.

To analyse these results it is important to emphasize that the ACT measurement corresponds to the displacement of the rails, while the LVDT measurement represents the vertical displacement of the slab. Therefore, it can be concluded that the vertical displacement of the rail, and therefore of the train

running on the track, depends mainly on the sleeper pad. On the other hand, the displacement of the slab will depend mainly on the Young's modulus of the FPL and of the subgrade.

Table 7 – Accelerations variation for -10% change in Young's Modulus

Layer	ACT_1	ACT_2	ACT_3	ACT_4	LVDT_1	LVDT_2	LVDT_3	LVDT_4
Rail	-0.02%	-0.02%	-0.02%	-0.02%	-0.01%	-0.01%	0.00%	0.00%
Rail pad	-10.64%	-10.63%	-10.60%	-10.60%	-0.01%	-0.01%	-0.01%	-0.01%
Slab	-0.07%	-0.07%	-0.09%	-0.09%	-0.08%	-0.08%	-0.09%	-0.08%
Grout	-0.01%	-0.01%	-0.02%	-0.02%	-0.06%	-0.06%	-0.05%	-0.05%
HBL	-0.04%	-0.04%	-0.06%	-0.06%	-0.49%	-0.49%	-0.49%	-0.50%
FPL	-0.26%	-0.26%	-0.25%	-0.25%	-6.96%	-6.96%	-6.97%	-6.97%
Subgrade	-0.12%	-0.12%	-0.15%	-0.15%	-3.36%	-3.36%	-3.32%	-3.32%

Table 8 – Accelerations variation for +10% change in Young's Modulus

Layer	ACT_1	ACT_2	ACT_3	ACT_4	LVDT_1	LVDT_2	LVDT_3	LVDT_4
Rail	-0.02%	-0.02%	-0.02%	-0.02%	-0.01%	-0.01%	0.00%	0.00%
Rail Pad	8.69%	8.69%	8.65%	8.65%	0.01%	0.01%	0.01%	0.01%
Slab	0.04%	0.04%	0.05%	0.05%	0.06%	0.07%	0.07%	0.07%
Grout	-0.01%	-0.01%	-0.01%	-0.01%	0.05%	0.05%	0.06%	0.06%
HBL	0.02%	0.02%	0.02%	0.02%	0.40%	0.41%	0.42%	0.42%
FPL	0.20%	0.20%	0.19%	0.18%	5.82%	5.82%	5.84%	5.84%
Subgrade	0.09%	0.09%	0.10%	0.10%	2.91%	2.91%	2.89%	2.89%

4.3. Poisson's Ratio

Table 9 and Table 10 show the percentage variation of accelerations when the Poisson's ratios of the model's layers change -10% and +10%, respectively. In these analyses, the rail pads are not included as they have been represented by spring elements, where Poisson's ratios is not applicable. The tables show that some variations in accelerations occur on FPL and subgrade. Considering the FPL, the accelerations decrease nearly 2% with a decrease of 10% in Poisson's ratio, at the LVDT positions, and they increase nearly 2.4% with the 10% increase in Poisson's ratio. Considering the subgrade, the decrease of accelerations is nearly 1.3%, at the LVDT positions, and increase about 1.7%, with the 10% decrease and increase in Poisson's ratio.

Table 9 – Accelerations variation for -10% change in Poisson's Ratio

Layer	ACT_1	ACT_2	ACT_3	ACT_4	LVDT_1	LVDT_2	LVDT_3	LVDT_4
Rail	-0.01%	-0.01%	-0.01%	-0.01%	0.00%	0.00%	0.01%	0.01%
Slab	-0.02%	-0.02%	-0.03%	-0.03%	-0.03%	-0.03%	-0.03%	-0.03%
Grout	-0.01%	-0.01%	-0.01%	-0.01%	0.00%	0.00%	0.01%	0.01%
HBL	-0.01%	-0.01%	-0.01%	-0.01%	0.02%	0.02%	0.03%	0.02%
FPL	-0.07%	-0.07%	-0.08%	-0.08%	-1.85%	-1.85%	-1.82%	-1.82%
Subgrade	-0.05%	-0.05%	-0.07%	-0.07%	-1.33%	-1.33%	-1.29%	-1.29%

Table 10 – Accelerations variation for +10% change in Poisson's Ratio

Layer	ACT_1	ACT_2	ACT_3	ACT_4	LVDT_1	LVDT_2	LVDT_3	LVDT_4
Rail	-0.01%	-0.01%	-0.01%	-0.01%	0.00%	0.00%	0.01%	0.01%
Slab	0.00%	0.00%	0.00%	0.00%	0.03%	0.03%	0.03%	0.03%
Grout	-0.01%	-0.01%	-0.01%	-0.02%	0.00%	0.00%	0.01%	0.01%
HBL	-0.01%	-0.01%	-0.02%	-0.02%	-0.02%	-0.02%	-0.01%	-0.02%
FPL	0.06%	0.06%	0.07%	0.07%	2.38%	2.38%	2.37%	2.37%
Subgrade	0.04%	0.04%	0.05%	0.05%	1.74%	1.74%	1.72%	1.72%

5. Summary and Conclusions

The present work concerns itself with the development of numerical tools for the analysis of railway infrastructures based on the understanding that accurate numerical solutions are key elements for the improvement of railways systems. High speed lines safety and comfort depend on good design practices, which must rely on accurate computational modelling. In turn, well-designed railway tracks will lead to lower track and vehicle maintenance costs.

This work develops reliable 3D FE models for a slab track system based on full-scale laboratory tests. The slab track system is composed of rails, rail pads, slab track, grout, HBL, FPL and subgrade. The slab track experimental tests have been performed in a full-scale testing facility. The tests are conducted to simulate actual loading conditions that tracks are subjected to during railway operations. Rail pads have been tested at LADICIM laboratory, University of Cantabria, and the results provide very useful input for the numerical models developed in this work.

The 3D slab track is modelled with the FE method aiming to reproduce displacement and acceleration results obtained from the experimental tests. As the actual values of some of the material properties of the track system are uncertain, reference values from the specialized literature are used. The FE model is then calibrated through mesh refinement studies and material parameters adjustment. Further, a parametric analysis is performed varying the values of density, Young's modulus and Poisson's ratio in order to establish the material properties to which the model behaviour is more sensitive. It has been found that the Young's modulus is the property that has greater effect on the numerical models, in particular for the rail pads, FPL and subgrade. This indicates that the definition of this property should be performed accurately as it is very important for the behaviour of the whole track system.

Future extensions of this work include the use of the calibrated track model developed here to study the track performance when interacting with railway vehicles using co-simulation approaches to handle the wheel-rail contact problem. Further, the model can be employed to compare the performance of slab track technology with other track solutions, e.g., ballast and asphalt. Finally, the calibrated model can be useful in several other investigations such as the development of tracks failure criteria procedures, vehicle structural behaviour, and track and vehicle life cycle assessments.

Acknowledgements

The first author would like to thank Pontificia Universidade Catolica do Parana (PUCPR), Heriot-Watt University and LADICIM for making all this work possible. Also, she would like to thank CAPES for the doctoral scholarship, and also for the scholarship of the *Programa de Doutorado Sanduíche no Exterior - PDSE*, which allowed her stay at Heriot-Watt University. This work was supported by the Portuguese Foundation for Science and Technology, through IDMEC, under LAETA, project UIDB/50022/2020.

References

[1] Gourvish T. The High Speed Rail Revolution: History and Prospects. HS2 Ltd 2010.

[2] Esveld C. Modern Railway Track. MRT Prod 2001.

[3] Voivret C, Nhu V-H, Peralès R. Discrete Element Method Simulation as a Key Tool Towards Performance Design of Ballasted Tracks. Int J Railw Technol 2016;5:83–98. doi:10.4203/ijrt.5.1.4.

[4] Peltokangas O, Nurmikolu A. Evolution of Railway Track Settlement after Ballast Tamping. Int J Railw Technol 2015;4:1–18. doi:10.4203/ijrt.4.2.1.

[5] Costa D'Aguiar S, Arlaud E, Potvin R, Laurans E, Funfschillling C. Railway Transitional Zones: A Case History from Ballasted to Ballastless Track. Int J Railw Technol 2014;3:37–61. doi:10.4203/ijrt.3.1.2.

[6] Sañudo R, Markine V, Pombo J. Study on Different Solutions to Reduce the Dynamic Impacts in Transition Zones for High-Speed Rail. J Theor Appl Vib Acoust 2017;3:199–222. doi:10.22064/tava.2018.80091.1095.

[7] Woodward PK, Kennedy J, Laghrouche O, Connolly DP, Medero G. Study of railway track stiffness modification by polyurethane reinforcement of the ballast. Transp Geotech 2014;1:214–24. doi:10.1016/j.trgeo.2014.06.005.

[8] Steenbergen MJMM, Metrikine AV, Esveld C. Assessment of design parameters of a slab track railway system from a dynamic viewpoint. J Sound Vib 2007;306:361–71. doi:10.1016/J.JSV.2007.05.034.

[9] Sainz-Aja J, Pombo J, Tholken D, Carrascal I, Polanco J, Ferreño D, et al. Dynamic calibration of slab track models for railway applications using full-scale testing. Comput Struct 2020;228:106180. doi:10.1016/j.compstruc.2019.106180.

[10] Bian X, Jiang H, Cheng C, Chen Y, Chen R, Jiang J. Full-scale model testing on a ballastless high-speed railway under simulated train moving loads. Soil Dyn Earthq Eng 2014;66:368–84. doi:10.1016/j.soildyn.2014.08.003.

[11] Sainz-Aja J, Carrascal I, Polanco JA, Thomas C, Sosa I, Casado J, et al. Self-compacting recycled aggregate concrete using out-of-service railway superstructure wastes. J Clean Prod 2019;230:945–55. doi:10.1016/j.jclepro.2019.04.386.

[12] Fang M, Park D, Singuranayo JL, Rose JG. A Numerical Study on Asphalt Layer Location in a Slab Track System for High-Speed Railways. Int J Railw Technol 2017;6:23–39. doi:10.4203/ijrt.6.1.2.

[13] Yu Z, Connolly DP, Woodward PK, Laghrouche O. Settlement behaviour of hybrid asphalt-ballast railway tracks. Constr Build Mater 2019;208:808–17. doi:10.1016/j.conbuildmat.2019.03.047.

[14] Nguyen K, Goicolea JM, Galbadon F. Dynamic effect of high speed railway traffic loads on the ballast track settlement. Congr Métodos Numéricos Em Eng 2011.

[15] Bosso N, Gugliotta A, Zampieri N. A Comprehensive Strategy to Estimate Track Condition and its Evolution. Int J Railw Technol 2012;1:1–19. doi:10.4203/ijrt.1.2.1.

[16] Indraratna B, Nimbalkar S, Rujikiatkamjorn C. Modernisation of Rail Tracks for Higher Speeds and Greater Freight. Int J Railw Technol 2013;2:1–20. doi:10.4203/ijrt.2.3.1.

[17] Fortunato E, Paixão A, Calçada R. Railway Track Transition Zones: Design, Construction, Monitoring and Numerical Modelling. Int J Railw Technol 2013;2:33–58. doi:10.4203/ijrt.2.4.3.

[18] Mezher SB, Connolly DP, Woodward PK, Laghrouche O, Pombo J, Costa PA. Railway critical velocity – Analytical prediction and analysis. Transp Geotech 2016;6:84–96. doi:10.1016/j.trgeo.2015.09.002.

[19] Momoya Y, Nakamura T, Fuchigami S, Takahashi T. Improvement of Degraded Ballasted Track to Reduce Maintenance Work. Int J Railw Technol 2016;5:31–54. doi:10.4203/ijrt.5.3.2.

[20] Woodward PK, Laghrouche O, Mezher SB, Connolly DP. Application of Coupled Train-Track Modelling of Critical Speeds for High-Speed Trains using Three-Dimensional Non-Linear

Finite Elements. Int J Railw Technol 2015;4:1–35. doi:10.4203/ijrt.4.3.1.
[21] Cai Z, Raymond GP. Modelling the dynamic response of railway track to wheel/rail impact loading. Struct Eng Mech 1994;2:95–112. doi:10.12989/sem.1994.2.1.095.
[22] Costa J, Antunes P, Magalhães H, Ambrósio J, Pombo J. Development of Flexible Track Models for Railway Vehicle Dynamics Applications. Civil-Comp Proc., vol. 110, 2016. doi:10.4203/ccp.110.98.
[23] Poveda E, Yu RC, Lancha JC, Ruiz G. A numerical study on the fatigue life design of concrete slabs for railway tracks. Eng Struct 2015;100:455–67. doi:10.1016/j.engstruct.2015.06.037.
[24] Correia dos Santos N, Barbosa J, Calçada R, Delgado R. Track-ground vibrations induced by railway traffic: experimental validation of a 3D numerical model. Soil Dyn Earthq Eng 2017;97:324–44. doi:10.1016/j.soildyn.2017.03.004.
[25] Ferreira PA, López-Pita A. Numerical modelling of high speed train/track system for the reduction of vibration levels and maintenance needs of railway tracks. Constr Build Mater 2015;79:14–21. doi:10.1016/j.conbuildmat.2014.12.124.
[26] Azoh TS, Djeumako B, Fotsing BS. Modelling of train track vibrations for maintenance perspectives: application. Eur Sci J 2014;10:260–75. doi:10.19044/esj.2014.v10n21p%25p.
[27] Zhai W, Cai Z. Dynamic interaction between a lumped mass vehicle and a discretely supported continuous rail track. Comput Struct 1997;63:987–97. doi:10.1016/S0045-7949(96)00401-4.
[28] Huang H, Chrismer S. Discrete element modelling of ballast settlement under trains moving at "critical Speeds." Constr Build Mater 2013. doi:10.1016/j.conbuildmat.2012.09.007.
[29] Nguyen K, Goicolea JM, Galbadón F. Comparison of dynamic effects of high-speed traffic load on ballasted track using a simplified two-dimensional and full three-dimensional model. Proc Inst Mech Eng Part F J Rail Rapid Transit 2014;228:128–42. doi:10.1177/0954409712465710.
[30] Sainz-Aja J, Carrascal I, Ferreño D, Pombo J, Casado J, Diego S. Influence of the operational conditions on static and dynamic stiffness of rail pads. Mech Mater 2020;148:103505. doi:10.1016/j.mechmat.2020.103505.
[31] Antunes P, Magalhães H, Ambrósio J, Pombo J, Costa J. A co-simulation approach to the wheel–rail contact with flexible railway track. Multibody Syst Dyn 2019;45:245–72. doi:10.1007/s11044-018-09646-0.
[32] Pombo J, Almeida T, Magalhães H, Antunes P, Ambrósio J. Finite Element Methodology for Flexible Track Models in Railway Dynamics Applications. Int J Veh Struct Syst 2013;5. doi:10.4273/ijvss.5.2.01.
[33] Costa J, Antunes P, Magalhães H, Pombo J, Ambrósio J. A Novel Methodology to Automatically Include General Track Flexibility in Railway Vehicle Dynamic Analyses. Inst Mech Eng Part F, J Rail Rapid Transit 2020.
[34] Costa J, Antunes P, Magalhães H, Pombo J, Ambrósio J. A Finite Element Methodology to Model Flexible Tracks with Arbitrary Geometry for Railway Dynamics Applications. Comput Struct 2020.
[35] Pombo J, Ambrosio J. Modelling Tracks for Toller Coaster Dynamics. Int J Veh Des 2007;45:470. doi:10.1504/IJVD.2007.014916.
[36] Sequeira B, Pombo J, Antunes P, Ambrósio J, Woodward P. Construction of Three-Dimensional Track Models for Roller-Coaster Applications. Civil-Comp Proc., vol. 110, 2016. doi:10.4203/ccp.110.99.
[37] Sequeira B, Pombo J, Antunes P, Ambrósio J, Woodward P. Development of a Methodology for the Geometric Parameterization of Three-Dimensional Tracks. Civil-Comp Proc., vol. 108, 2015. doi:10.4203/ccp.108.133.
[38] Muñoz S, Aceituno JF, Urda P, Escalona JL. Multibody model of railway vehicles with weakly coupled vertical and lateral dynamics. Mech Syst Signal Process 2019;115:570–92. doi:10.1016/j.ymssp.2018.06.019.
[39] Pombo J, Ambrósio J, Silva M. A new wheel–rail contact model for railway dynamics. Veh Syst Dyn 2007;45:165–89. doi:10.1080/00423110600996017.

[40] Alonso A, Guiral A, Gimenez JG. Wheel Rail Contact: Theoretical and Experimental Analysis. Int J Railw Technol 2013;2:15–32. doi:10.4203/ijrt.2.4.2.
[41] Pombo J, Ambrósio J. Application of a wheel–rail contact model to railway dynamics in small radius curved tracks. Multibody Syst Dyn 2008;19:91–114. doi:10.1007/s11044-007-9094-y.
[42] Sichani MS, Enblom R, Berg M. Non-Elliptic Wheel-Rail Contact Modelling in Vehicle Dynamics Simulation. Int J Railw Technol 2014;3:77–96. doi:10.4203/ijrt.3.3.5.
[43] Marques F, Magalhães H, Pombo J, Ambrósio J, Flores P. A three-dimensional approach for contact detection between realistic wheel and rail surfaces for improved railway dynamic analysis. Mech Mach Theory 2020;149:103825. doi:10.1016/j.mechmachtheory.2020.103825.
[44] Magalhães H, Marques F, Liu B, Antunes P, Pombo J, Flores P, et al. Implementation of a non-Hertzian contact model for railway dynamic application. Multibody Syst Dyn 2019. doi:10.1007/s11044-019-09688-y.
[45] Pombo J, Ambrosio J. A Computational Efficient General Wheel-Rail Contact Detection Method. J Mech Sci Technol 2005;19:411–21. doi:10.1007/BF02916162.
[46] Marques F, Magalhães H, Liu B, Pombo J, Flores P, Ambrósio J, et al. On the generation of enhanced lookup tables for wheel-rail contact models. Wear 2019;434–435:202993. doi:10.1016/j.wear.2019.202993.
[47] Vollebregt EAH, Steenbergen MJMM. A Methodology for Assessing Track Irregularities with respect to Rail Damage. Int J Railw Technol 2015;4:85–105. doi:10.4203/ijrt.4.4.5.
[48] Pombo J, Ambrósio J. An alternative method to include track irregularities in railway vehicle dynamic analyses. Nonlinear Dyn 2012;68:161–76. doi:10.1007/s11071-011-0212-2.
[49] Hsu SS, Fagan N. Improving Switches and Crossings Performance and Reliability. Int J Railw Technol 2016;5:79–93. doi:10.4203/ijrt.5.3.4.
[50] Coleman I, Kassa E, Smith R. Wheel-Rail Contact Modelling within Switches and Crossings. Int J Railw Technol 2012;1:45–66. doi:10.4203/ijrt.1.2.3.
[51] Hölscher P. The Dynamics of Foundations for High Speed Lines on Soft Soils. Int J Railw Technol 2012;1:147–66. doi:10.4203/ijrt.1.1.7.
[52] Kuka N, Ariaudo C, Verardi R, Pombo J. Impact of Rail Infrastructure Maintenance Conditions on the Vehicle-Track Interaction Loads. Proc Inst Mech Eng Part C J Mech Eng Sci 2020.
[53] Iwnicki SD, Bevan AJ. Damage to Railway Wheels and Rails: A Review of the Causes, Prediction Methods, Reduction and Allocation of Costs. Int J Railw Technol 2012;1:121–46. doi:10.4203/ijrt.1.1.6.
[54] Pombo J. Application of a Computational Tool to Study the Influence of Worn Wheels on Railway Vehicle Dynamics. J Softw Eng Appl 2012;05:51–61. doi:10.4236/jsea.2012.52009.
[55] Stichel S, Jönsson P-A, Casanueva C, Hossein Nia S. Modelling and Simulation of Freight Wagon with Special attention to the Prediction of Track Damage. Int J Railw Technol 2014;3:1–36. doi:10.4203/ijrt.3.1.1.
[56] Kuka N, Verardi R, Ariaudo C, Pombo J. Impact of maintenance conditions of vehicle components on the vehicle–track interaction loads. Proc Inst Mech Eng Part C J Mech Eng Sci 2018;232:2626–41. doi:10.1177/0954406217722803.
[57] Magalhães H, Ambrósio J, Pombo J. Railway Vehicle Modelling for the Vehicle–Track Interaction Compatibility Analysis. Proc Inst Mech Eng Part K J Multi-Body Dyn 2016;230:251–67. doi:10.1177/1464419315608275.
[58] Rail One. Ballastless Track System Rheda 2000® - High Speed to Perfection. WwwRailoneCom 2020. https://www.railone.com/products-solutions/long-distance-and-freight-transport/ballastless-track-systems/rheda-2000r.
[59] Banimahd M. Advanced Finite Element Modelling of Coupled Train-Track Systems: A Geotechnical Perspective. PhD Dissertation, Heriot-Watt University, UK, 2008.
[60] Madhkhan M, Entezam M, Torki ME. Mechanical Properties of Precast Reinforced Concrete Slab Tracks on Non-Ballasted Foundations. Sci Iran 2012;19:20–6. doi:10.1016/j.scient.2011.11.037.
[61] Jang SY, Lee S-H, Kim YB, Kim E, Lee IW, Kang YS. Development of Prefabricated Concrete

Slab Track Systems and Trial Installation on Revenue Line. 8th World Congr Railw Res 2008.
[62] Bastin R. Development of German non-ballasted track forms. Proc. Inst. Civ. Eng., vol. 159, Thomas Telford Ltd; 2006, p. 25–39.
[63] Michas G. Slab Track Systems for High-Speed Railways. MSc Dissertation, KTH - Royal Institute of Technology, Sweden, 2012.
[64] Yang J, Kong B, Cai CS, Wang JS. Behavior of High-Speed Railway Ballastless Track Slabs Using Reactive Powder Concrete Materials. J Transp Eng 2016;142:04016031. doi:10.1061/(ASCE)TE.1943-5436.0000849.
[65] Zhu S, Cai C. Stress intensity factors evaluation for through-transverse crack in slab track system under vehicle dynamic load. Eng Fail Anal 2014;46:219–37. doi:10.1016/j.engfailanal.2014.09.004.
[66] Esveld C. Slab Track : A Competitive Solution. Esveld Consult 1999:1–5.
[67] Robertson I, Masson C, Sedran T, Barresi F, Caillau J, Keseljevic C, et al. Advantages of a new ballastless trackform. Constr Build Mater 2015;92:16–22. doi:10.1016/j.conbuildmat.2014.06.099.
[68] Marolt Čebašek T, Esen AF, Woodward PK, Laghrouche O, Connolly DP. Full scale laboratory testing of ballast and concrete slab tracks under phased cyclic loading. Transp Geotech 2018;17:33–40. doi:10.1016/j.trgeo.2018.08.003.
[69] Ferreño D, Casado J, Carrascal I, Diego S, Ruiz E, Saiz M, et al. Experimental and finite element fatigue assessment of the spring clip of the SKL-1 railway fastening system. Eng Struct 2019;188:553–63. doi:10.1016/j.engstruct.2019.03.053.
[70] Sainz-Aja J, Ferreño D, Carrascal I, Pombo J, Casado J, Diego S, et al. Prediction of Mechanical Properties of Rail Pads Under in-Service Conditions Through Machine Learning Algorithms. Adv Eng Softw 2020.